Applied Energy Symposium 2020: Low carbon cities and urban energy systems
October 10-17, 2020
Paper ID: CUE2020-D-059

An Experimental Study on Effects of Steady and Unsteady Heat Flux on Flow Boiling in Straight Microchannel

Jiaojiao Zhuang[1], Hao Yu[1], Ning Mao[1*]

1 Department of Gas Engineering, College of Pipeline and Civil Engineering, China University of Petroleum (East China), Qingdao, Shandong, China

ABSTRACT

The high heat flux on the PV cells can lead to the decrease of electricity efficiency. To tackle with the high temperature problems in PV cells microchannel is attracting increasing attentions recently due to its much higher heat flux. In this paper, the characteristics of flow boiling pressure drop and heat transfer of deionized water flow boiling in a microchannel with hydraulic diameter of 400 μm had been experimentally investigated. To further understand the effect of variation of solar radiation on cooling performance of the PV cells, unsteady and steady heat flux were respectively used and the corresponding pressure drop and heat dissipation of the microchannel under different mass fluxes (G=410.69, 513.36 and 718.71 kg/m^{2}s) were studied. It was found that with the increase of heat flux, the pressure drop first shows a slight downward trend, then increases sharply. The average heat transfer coefficient and local heat transfer coefficient increase with the increase of heat flux and decrease with the increase of mass flux. With the sudden increase of heat flux, a much longer variation of the pressure drop and wall temperature was observed.

Keywords: microchannel, flow boiling, pressure drop, heat transfer coefficient, unsteady heat flux

NONMENCLATURE

Abbreviations	
PTFE	polytetrafluoroethylene
Symbols	
P	pressure drop, KPa
h	heat transfer coefficient,
T	Temperature, °C
G	mass flux, kg/m^2s
q_{eff}	effective heat flux, KW/m^2
ρ	Density, kg·m^{-3}

1. INTRODUCTUON

The photovoltaic system has been widely used to generate clean electricity through converting solar energy into electricity[1]. However, the electricity conversion of PV cells is only around 10% and the most of the remaining solar energy is converted into heat which results in high temperature of PV panel [2]. It was reported that every 1 °C increase in temperature of PV panel leads to decrease of 0.2-0.5% electricity efficiency[2, 3]. Therefore, cooling of PV cell is quite important for maintaining the normal electricity efficiency [4]. To tackle with the high temperature problems in PV cells microchannel is attracting increasing attentions recently due to its much higher heat flux [5]. In past decades, number of studies have been carried out on the microchannel cooling or heat transfer properties.

Li[6] visualized the microchannels and studied the effects of mass flux and heat flux on the heat transfer coefficient and pressure drop. The experimental results show that the local heat transfer coefficient increases slightly with the increase of effective heat flux after the ONB. Besides, it can be seen that the heat transfer coefficient has a distinct increase tendency with the increase of mass flux. Yan[7] used R134a to conduct experiments of 0.5 mm × 0.5 mm × 45 mm in 30 parallel rectangular channels. The results show that the heat transfer coefficient increased with the mass flux, and presents an "M"-shaped curve with the increase of heat

* Corresponding author, Email: maoning@upc.edu.cn

flux. Under the same heat and mass flux conditions, the higher the saturation temperature, the lower the wall superheat and the higher the heat transfer coefficient. Harirchian[8] conducted a visualization experiment and found that the pressure drop and heat transfer coefficient increase with the increase of heat flux. Hedau[9] also found that the pressure drop and heat transfer coefficient increase with the growth of mass flux and heat flux. Kingston[10] studied the dynamic response of a heated 500 µm channel undergoing flow boiling of HFE-7100 is experimentally investigated for a single heat flux pulse through experiments. It is shown that longer duration high-heat-flux pulses can be withstood when the fluid in the microchannel is initial boiling, relative to if it is initially in the single-phase flow regime, despite being at an initially higher heat flux and wall temperature prior to the pulse.

These previous researches on flow boiling in microchannel provide a fundamental for the present study. However, most of the researches study the experimental microchannel flow boiling under stable heat flux, and rarely discuss experimental microchannel flow boiling under variable heat flux conditions. Since solar radiation was changing[11], the remaining solar heat on the PV cells also varies with the variation of solar radiation. Therefore, in this paper, a straight rectangular microchannel with hydraulic diameter of 400 µm was designed, and the flow boiling and heat transfer properties were experimentally investigated. To further understand the effect of variation of solar radiation on cooling performance of the PV cells, unsteady and steady heat flux were respectively used and the corresponding pressure drop and heat dissipation of the microchannel were studied.

2. Methodology

2.1. Experimental flow chart and apparatus

Fig.1 shows the experimental apparatus and flow chart. The experimental setup mainly comprised of a peristaltic pump, a power supply as heat source, an oil bath, a test section (microchannel), a high speed camera, and parameter measurement instrument, as shown in Fig. 1 and Fig. 2. The deionized (DI) water was used as working fluid. Before the experiment, deionized water was heated and boiled in a high-temperature heating pot to remove non-condensable gas. The cooled deionized water was driven by a constant flow peristaltic pump through a constant temperature oil bath and a flow meter reached the test section. After it was heated in the test section, it flows out into the water storage bottle. A damper was connected to the peristaltic pump to slow down the vibration. The constant temperature oil bath was used to regulate the inlet temperature for the microchannel. The test section consisted of microchannel part and heat source part. The heat was provided by the power supply, as shown in Fig. 1 and Fig. 2.

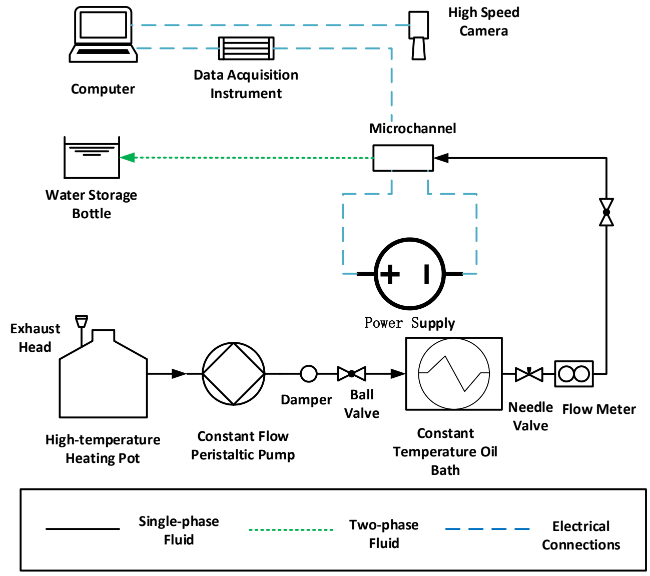

Fig.1 Schematic of flow chart and test section

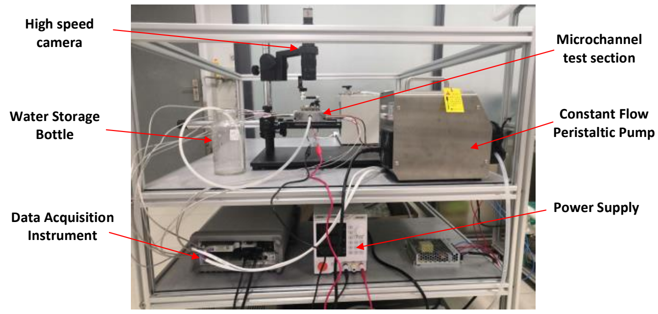

Fig. 2 Experiment setup and main components

Fig.3 shows the structure of the microchannel machined by copper. The channel dimension is 400 µm (width), 400 µm (depth) and 58 mm (length). The pressure at the inlet and outlet was measured by the pressure sensor. The inlet and outlet temperature of DI water and wall temperature were measured by k type thermocouples. The wall temperature measurement points are shown in Fig.3.

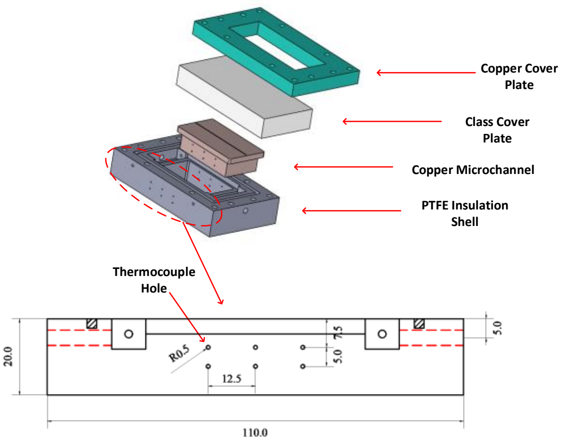

Fig.3 Structure diagram of the microchannel

2. 2 Experimental procedure

Due to the natural convection and radiation heat exchange between the experimental section and the surrounding air, the input heat flux density of the experimental section cannot be used to calculate the heat absorbed by the working fluid. Hence, there is a certain amount of heat dissipation that should be estimated. Therefore, a series of single-phase experiments with the same range of flow rate as flow boiling (two phase flow) type has been conducted to calculate the efficiency of heat supply to the microchannel. The heat efficiency was calculated at approximately 65% which was used in the following study.

The mass flux was controlled by the peristaltic pump in the range of 410.69 to 718.71 kg/m^{2}s. After the microchannel inlet temperature and mass flux were stable, the power supply was adjusted to provide the effective heat flux with the range of 238 to 624 kw/m^2. Therefore, the expected two-phase flow boiling conditions can be obtained.

2. 3 Data reduction

Heat flux was divided into input heat flux and effective heat flux, where the input heat flux q defined as,

$$q = \frac{Q_{tot}}{A_w} \tag{1}$$

Where Q_{tot} was the total input DC power heating power of the experimental section, KW; A_w was the heating area of the microchannel , m^2.

Q_{tot} was defined as，

$$Q_{tot} = \frac{V \times I}{1000} \tag{2}$$

Where V was the input voltage, V; I was the input current, A.

Due to the natural convection and radiation heat exchange between the experimental section and the surrounding air, there was a certain amount of heat dissipation. Therefore, through a series of single-phase heat balance experiments in the same flow range as the flow boiling (two-phase flow) type, the average efficiency $\bar{\eta}$ was obtained.

$$\bar{\eta} = \frac{1}{n}\sum_i^n \eta_i \tag{3}$$

$$\eta_i = \frac{Q_{net,i}}{Q_{tot,i}} \tag{4}$$

$$Q_{net,i} = c_p \dot{m}(T_{l,out} - T_{in}) \tag{5}$$

Where $Q_{net,i}$ was the heat absorbed by the fluid flowing through the experimental section per unit time in the experiment , kj/s.

q_{eff} was defined as,

$$q_{eff} = \bar{\eta} \times q \tag{6}$$

Microchannel pressure drop was equal to measured pressure drop minus the loss of the test section,

$$\Delta P_{\exp} = \Delta P_{in} - \Delta P_{out} \tag{7}$$

$$\Delta P = \Delta P_{\exp} - (\Delta P_{cont} + \Delta P_{\exp a}) \tag{8}$$

Where ΔP_{exp} was the measured pressure drop, pressure loss includes inlet contraction loss (ΔP_{cont}) and outlet expansion recovery (ΔP_{expa}), KPa;

ΔP_{cont} was defined as，

$$\Delta P_{cont} = \frac{G^2}{2\upsilon_f}\left[1 - \left(\frac{A_2}{A_1}\right)^2 + \frac{1}{2}\left(1 - \frac{A_2}{A_1}\right)^2\right] \tag{9}$$

Where υ_f was the liquid relative volume of the inlet working fluid, m³/kg; A_1 was the sum of cross-sectional area of inlet and outlet of test section, A_2 was the sum of the cross-sectional area of the inlet and outlet of the microchannel , m^2; G was the mass flux,kg/m^2s;

ΔP_{exp} was defined as，

$$\Delta P_{\exp a} = \frac{G^2}{\rho_l}\left[1+\frac{x_{out}\left(\rho_l-\rho_v\right)}{\rho_v}\right]\left[\frac{A_2}{A_1}-\left(\frac{A_2}{A_1}\right)^2\right] \quad (10)$$

Where ρ_l and ρ_v were the density of working fluid liquid and gas respectively, kg/m³;x_{out} was the thermodynamic equilibrium dryness at the outlet, defined as，

$$x_{out} = \frac{h_{out}-h_l}{h_{fg}} \quad (11)$$

Where h_l was the saturated liquid phase enthalpy (kJ/kg); h_{fg} was the latent heat of vaporization (kJ/kg) ; h_{out} was the enthalpy of the working fluid at the outlet of the microchannel, defined as，

$$h_{out} = \frac{q_{eff}A_w}{GA_c}+h_{in} \quad (12)$$

Where q_{eff} was the effective heat flux, KW/m^2; h_{in} was the enthalpy of the working fluid at the inlet of the microchannel (kJ/kg); A_c was the cross-sectional area of the microchannel.

When deionized water enters the microchannel to flow and exchange heat, the channel was divided into two regions: (1) super-cooled area of length L_{sub}; Saturated region of length $L-L_{sub}$,

$$L_{sub} = \frac{\dot{m}c_p\left(T_{sat}\left(Z,sub\right)-T_i\right)}{q_{eff}\left(2H+W\right)} \quad (13)$$

$$P_{sat}\left(Z_{sub}\right) = p_i - \frac{2f_{app}G^2}{\rho_l D_h}L_{sub} \quad (14)$$

$$f_{app} = 12.55Re^{-0.92} \quad (15)$$

Where $T_{sat}(Z,sub)$ was the saturation temperature at the end of the super-cooled area, T_i was the inlet temperature, °C； H was the height of the microchannel，W was the width of the microchannel，m ； $P_{sat}(Z_{sub})$ was the saturation pressure corresponding to the saturation temperature $T_{sat}(Z,sub)$，p_i was the inlet pressure，Pa；f_{app} was the apparent coefficient of friction，use the equations proposed in the literature[12] to predict.

The heat transfer coefficient of single-phase flow in the super-cooled zone was defined as,

$$h_{sp} = \frac{q_{eff}}{T_w\left(Z\right)-T_f\left(Z\right)} \quad (16)$$

T_w was the bottom temperature of the channel, defined as,

$$T_w = T_{mi} - \frac{q_{eff}e}{k} \quad (17)$$

Where T_{mi} was the temperature at the temperature measurement point closest to the bottom of the microchannel, °C; e was the distance between the temperature measurement point and the bottom of the microchannel, m; k was the thermal conductivity of copper, $\mathrm{w/mK}$.

$T_f(Z)$ was the fluid temperature from the microchannel entrance Z, defined as,

$$T_f\left(Z\right) = T_f\left(0\right) + \frac{2q_{eff}\left(W+2H\right)Z}{c_pGA_c} \quad (18)$$

The heat transfer coefficient of two-phase flow in the saturation region was defined as,

$$h_{tp} = \frac{q_{eff}}{T_w\left(Z\right)-T_{sat}\left(Z\right)} \quad (19)$$

3. Results and discussion

3.1Time average variation analysis of pressure drop

Fig.4 shows the changing of experimental pressure drop with heat flux at three constant mass fluxes of G=410.69, 513.36 and 718.71 kg/m^{2}s when the inlet temperature reaches 50 °C and 55 °C. It can be seen that for the same mass flux, as the heat flux increases, the pressure drop first shows a slight downward trend, and then rises sharply, the maximum pressure drop can reach 15.35kPa. With the increase of heat flux, the temperature of liquid phase in the channel increases, and the dynamic viscosity of liquid phase decreases, which leads to the slight decrease of flow resistance and pressure drop. However, when the heat flux increases to a certain value, water vapor generated, which leads to the increase in pressure drop, as shown in Fig. 4. With the continuous increase of heat flux, the fraction of water vapor was increased sharply, which therefore promote the obviously rapid increase in pressure drop, as shown in Fig. 4. At low heat fluxes, and only liquid flows in the microchannel, the pressure drop of the high mass flux is significantly higher than that of the lower one, which is the result of a combination of larger dynamic viscosity and mass flux. And mass flux plays a dominant role in experimental pressure drop. With the increase of the heat flux, the vapor is generated in the microchannel. The relationship between the pressure drop of low mass flux and that of high mass flux is reversed, which indicates that the frictional pressure drop and accelerated pressure drop caused by the vapor generation play a dominant role in the experimental pressure drop.

For different inlet temperature, the trends of pressure drop with the increase of heat flux are similar, as shown in Fig. 4(a) and (b). For T_{in}=55 °C, the pressure drop is slightly smaller than that of T_{in}=50 °C. This was due to the lower dynamic viscosity at the full liquid phase flow section. However, at high inlet temperature, the differences of pressure drop between the three mass flux cases in the saturated region were enlarged because of the increase in amount of vapor.

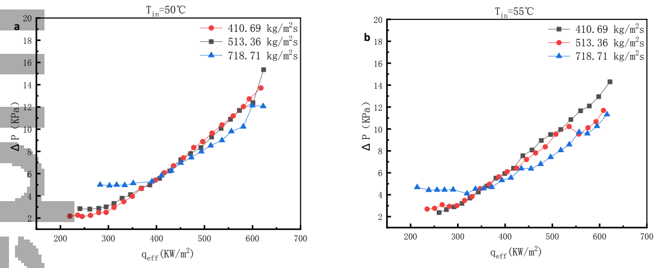

(a) T_{in}=50 °C (b) T_{in}=55 °C

Fig.4 Variation of pressure drop versus heat flux under different mass flux

3.2 Time average variation analysis of heat transfer coefficient

The influence of heat flux on average heat transfer coefficient and local heat transfer coefficient in boiling zone (z=41.5mm) at different mass flux (G=410.69, 513.36 and 718.71 kg/m^{2}s) and inlet temperature (T_{in}=50 °C and T_{in}=55 °C) is displayed in Fig.5 and Fig.6. It can be seen that the average heat transfer coefficient and local heat transfer coefficient showed a rising trend with increasing heat flux. With the heat flux increases, the transition from the single-phase to the two-phase occurred in the microchannel, and the two-phase area increases, hence, the average heat transfer coefficient increases, as shown in Fig. 5, when the inlet temperature is 55℃ and the mass flux is 410.69kg/m^{2}s, the heat transfer coefficient changes the most. With the increase of heat flux, the heat transfer coefficient increases from 16.41 kw/m^{2}K to 65.59 kw/m^{2}K. The vapor generation rate increases with increasing heat flux due to enhanced nucleate boiling, which results in the average heat transfer coefficient and local heat transfer coefficient to increase for the same mass flux conditions.

It is interesting to noted that the average heat transfer coefficient and local heat transfer coefficient decrease with the increase of mass flux. And the highest mass flux corresponds to the lowest heat transfer coefficient in the experimental heat flux range. It can be explained that under certain heat flux conditions, the amount of vapor is bigger at a lower mass flux and the average heat transfer coefficient and local heat transfer coefficient increases significantly. Therefore, compared with the mass flux, the vapor generation is the main factor to increase the average heat transfer coefficient and local heat transfer coefficient.

For different inlet temperatures, the average heat transfer coefficient at different flow flux shows similar behavior with the increase of heat flux. The maximum average heat transfer coefficient when the inlet temperature is 55°C is 12.29KW/m^{2}K higher than the maximum average heat transfer coefficient when the inlet temperature is 50°C.However, the local heat transfer coefficient is different from the former. With increasing heat flux, the values of the local heat transfer coefficient for different mass fluxes are closer at high inlet temperature. That means the local heat transfer coefficient tends not to depend on mass flux. It also reflects the character of nucleate boiling heat transfer.

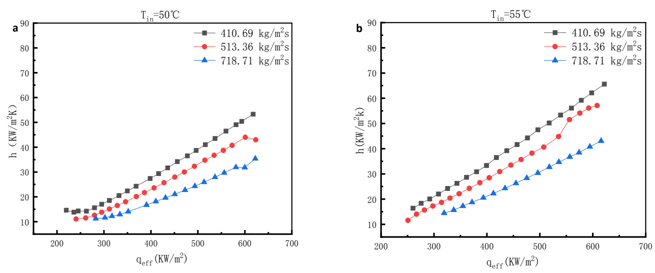

Fig.5 Variation of average heat transfer coefficient versus heat flux under different mass flux

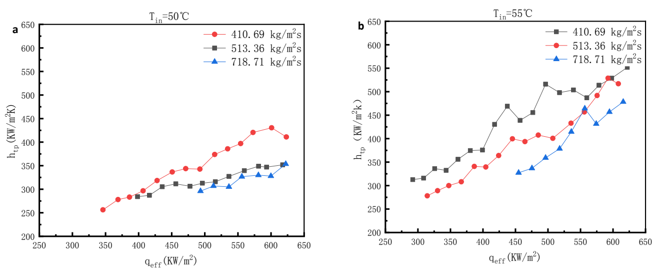

Fig.6 Variation of local heat transfer coefficient versus heat flux under different mass flux

3.3 Pressure drop and heat characteristics under *unsteady heating conditions*

The impact of transient heating conditions on pressure drop for the heat power pulse from 36.3W to 57.7W is illustrated in Fig.7. The heat power pulse started at 0s. The heat power increased rapidly to about 53.6W in two seconds and gradually reached 57.7W in the following 42 seconds. The resistance of the heating plate changes with its own temperature so that the pulse time is long. When the heating power is 36.3W, the pressure drop is 4.34KPa. With the sudden increase of heat flux, the pressure drop begin to rise at 20s until it reaches 9.27 KPa around 60s and starts to stabilize. With the sudden increase of heat flux, the pressure drop begin to rise at 20s until it starts to stabilize at about 60s. The reason for the phenomenon is that with heat flux growing sharply, the vapor generated dramatically. Therefore, the experimental pressure drop will raise rapidly because of the two-phase frictional pressure drop and vapor-phase accelerated pressure drop. Fig.8 shows the wall temperature as a function of time under the transient heating conditions. When the heating power is 36.3W, the wall temperature is 100.58°C. With the sudden increase of heat flux, the wall temperature starts to increase quickly at about 10s until it reaches 102.8 °C, which aggravates the boiling in the single microchannel. This variation corresponds to the dynamic response of pressure drop with the dramatic variation of the heat power in Fig.7.

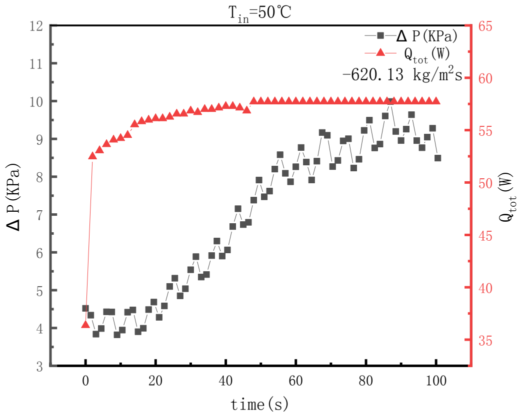

Fig.7 Synchronized measurements of power and pressure drop as a function of time

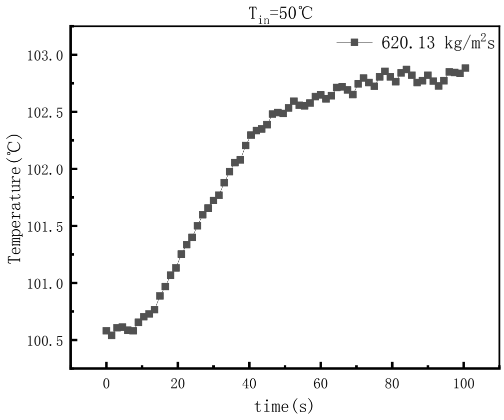

Fig.8 Wall temperature variation with time

4. CONCLUSIONS

This paper presented an experimental investigation on the characteristics of deionized water flow boiling in straight rectangular microchannel with channel hydraulic diameter of 400 μm. The effects of mass flux rate, inlet temperature, heat flux, and unsteady heat flux on the pressure drop and heat dissipation of the microchannel were studied. The main conclusions can be summarized as:

(1) With the increase of heat flux, the pressure drop of three different mass fluxes (G=410.69, 513.36 and 718.71 kg/m^{2}s) first shows a slight downward trend, then increases sharply. At low heat fluxes, the pressure drop of the high mass flux (like G=718.71 kg/m^{2}s) is significantly higher than that of the lower one (like G=410.69 kg/m^{2}s). The relationship between the pressure drop of low mass flux and that of high mass flux is reversed at high heat fluxes.

(2) The average heat transfer coefficient and the local heat transfer coefficient (z=41.5mm) increases with the increase of heat flux from 219.79KW/m^2 to 623.18 KW/m^2 and decreases with the increase of mass flux from 410.69 kg/m^{2}s to 718.71 kg/m^{2}s. At different inlet temperatures (T_{in}=50 °C and T_{in}=55 °C), the average heat transfer coefficients at different fluxes show similar behavior with the increase of heat flux. With increasing heat flux, the values of the local heat transfer coefficient for different mass fluxes (G=410.69, 513.36 and 718.71 kg/m^{2}s) are closer at 55°C inlet temperature.

(3) With the sudden increase of heat flux and the heat power pulse from 36.3W to 57.7W quickly, the pressure drop increases 4.97KPa and wall temperature rises from 100.58°C to 102.8 °C until it

stabilizes. The reason for the phenomenon is that with heat flux growing sharply, the vapor generated dramatically.

ACKNOWLEDGEMEN

The study was supported by the Shandong Provincial Natural Science Foundation, China (Project No.: ZR2016EEQ29) and the Fundamental Research Funds for the Central Universities (No.: 18CX02077A).

REFERENCE

[1] Zhao J, Song Y, Lam WH, et al. Solar radiation transfer and performance analysis of an optimum photovoltaic/thermal system. Energy Conversion & Management, 2011, 52(2): 1343-1353.

[2] Ali HM. Recent advancements in PV cooling and efficiency enhancement integrating phase change materials based systems – A comprehensive review. Solar Energy, 2020, 197: 163-198.

[3] King DL, Eckert PE. 1996. Characterizing (Rating) the performance of large photovoltaic arrays for all operating conditions. Twenty Fifth IEEE Photovoltaic Specialists Conference - Washington, DC, USA, 1996, 1385-1388.

[4] Valeh-E-Sheyda P, Rahimi M, Karimi E, et al. Application of two-phase flow for cooling of hybrid microchannel PV cells: A comparative study. Energy Conversion & Management, 2013, 69: 122-130.

[5] Sohel Murshed SM, de Castro CA. A critical review of traditional and emerging techniques and fluids for electronics cooling. Renew Sust Energ Rev, 2017; 78: 821-833.

[6] Li YF, Xia GD, Ma DD, et al. Experimental investigation of flow boiling characteristics in microchannel with triangular cavities and rectangular fins[J]. International Journal of Heat and Mass Transfer, 2019, 148: 119036.

[7] Yan Q, Jia L, An Z, et al. A comprehensive criterion for slug-annular flow transition based on flow boiling of R134a in microchannels. International Communications in Heat & Mass Transfer, 2019, 105: 1-9.

[8] Harirchian T, Garimella S V. The critical role of channel cross-sectional area in microchannel flow boiling heat transfer. International Journal of Multiphase Flow, 2009, 35(10): 904-913.

[9] Hedau G, Dey P, Raj R, et al. Experimental and numerical investigation of the effect of number of parallel microchannels on flow boiling heat transfer. International Journal of Heat and Mass Transfer, 2020, 158: 119973.

[10] Kingston TA, Weibel JA, Garimella SV. Time-resolved characterization of microchannel flow boiling during transient heating: Part 1 – Dynamic response to a single heat flux pulse. International Journal of Heat and Mass Transfer, 2020, 154: 119686.

[11] Wang Z, Wei J, Zhang G, et al. Design and performance study on a large-scale hybrid CPV/T system based on unsteady-state thermal model. Solar Energy, 2019, 177: 427-439.

[12] Mirmanto M. Flow and Heat Transfer in Horizontal Rectangular Microchannels. Scholars' Press， 2014.